

RESEARCH ARTICLE

In silico screening of *Annona muricata* L. leaf constituents and derivatives towards selected Type 2 Diabetes Mellitus - related protein targets

David John T. Jarillo*¹, Vince Lambert H. Padilla¹, Junie B. Billones²

*Corresponding author's email address: dtjarillo@up.edu.ph

¹Department of Pharmaceutical Chemistry, College of Pharmacy, University of the Philippines Manila, Manila, Philippines

²Department of Physical Sciences and Mathematics, College of Arts and Sciences, University of the Philippines Manila, Manila, Philippines

ABSTRACT

Background: Type 2 diabetes mellitus, or T2DM, is one of the world's most chronic health problems that is linked to numerous deaths and high health care expenses. 11 β -hydroxysteroid dehydrogenase type 1 (11 β -HSD1), protein-tyrosine phosphatase 1B (PTP1B) and mono-ADP-ribosyl transferase sirtuin-6 (SIRT6) were among the novel proteins and focus targets of diabetes research. *Annona muricata* is a commonly used natural remedy for several illnesses, including type 2 diabetes mellitus. However, most of these traditional claims have received few molecular evaluations.

Objectives: This study investigated the phytoconstituents and derivatives of the leaves of *A. muricata* by evaluating their binding affinities towards selected novel T2DM-related protein targets through *in silico* methods.

Methodology: This study screened the potential lead compounds from the leaves of *A. muricata* by evaluating the binding energies (kcal/mol) of the parent compounds and derivatives with the targets compared to the native ligands and known substrates through molecular docking.

Results: The 8 parent compounds – the alkaloids coreximine and isolaureline, and phenolic compounds chlorogenic acid, epicatechin, kaempferol, kaempferol 3-O-rutinoside, quercetin, and rutin were selected for bioisosteric modifications. Furthermore, after docking simulations of derivatives, compounds ACM018, ACM021, ACM024, ACM036, and ACM044, are the top 5 derivatives for 11 β -HSD1. In PTP1B, ACM014, ACM020, ACM021, ACM024, and ACM028 are the top 5 ligands. Lastly, BCM008, BCM022, DCM004, DCM025, and DCM027 are the top 5 derivatives for SIRT6.

Conclusion: Based on the binding energies of the parent compounds and derivatives, they exhibited comparable binding affinity as the controls. Moreover, the designed derivatives may be synthesized and further investigated for potential biological effects towards 11 β -HSD1, PTP1B, and SIRT6 through *in vitro* and *in vivo* experiments.

Keywords: *Annona muricata*, Type 2 Diabetes Mellitus, *In silico* methods, Alkaloids, Phenolic compounds

Introduction

Annona muricata (Annonaceae) or locally known as Guyabano in the Philippines, is a commonly used natural remedy for several illnesses, including type 2 diabetes mellitus. The bioactivities and therapeutic effects of this medicinal plant have been extensively studied [1]. A variety of foreign and local studies have demonstrated that *Annona muricata* leaves offer several potential pharmacological activities such as hypoglycemic effects [2,3], antibacterial [4], antifungal [5], antimalarial [6], antimutagenic [7], anticonvulsant [8], sedative [9] and insecticidal [10].

Diabetes mellitus (DM) is a chronic disease where the blood glucose concentration of a patient is consistently high. Among the types of DM, type 2 diabetes mellitus (T2DM) is the most significant contributor to the burden of diabetes globally, accounting for up to 90% of all cases of diabetes worldwide [11]. It is primarily characterized by two factors: defective insulin secretion and the inability of insulin-sensitive tissues to properly respond to insulin [12]. Due to its complex pathogenesis, novel targets have emerged and become the focus of diabetes research [13,14].

11 β -hydroxysteroid dehydrogenase type I (11 β -HSD1) is a nicotinamide adenine dinucleotide phosphate (NADPH)-dependent enzyme that is vastly expressed in human tissues, specifically in fat and liver tissues, and is responsible for the conversion of cortisone to its active form cortisol, which is necessary for homeostasis regulation [15]. Glucocorticoids such as cortisol oppose the primary effect of insulin, which is to increase glucose uptake [16]. Increased tissue activity of 11 β -HSD1 may result in increased intracellular cortisol levels, resulting in metabolic changes such as insulin resistance, promotion of gluconeogenesis, impaired insulin signaling and increased hepatic glucose [16]. The inhibition of 11 β -HSD1 is a viable target for the therapy of glucocorticoid-associated conditions, particularly T2DM [17,18].

Protein-tyrosine phosphatase 1B (PTP1B) has been recognized to negatively regulate the insulin signaling pathway [19]. PTP1B is responsible for insulin receptor desensitization that has been associated with the development of insulin resistance. It regulates this process by dephosphorylating phospho-tyrosine residues in the tissue insulin receptor kinase, halting the entire insulin action process. PTP1B inhibition may prolong insulin receptor activity; therefore, it has emerged as a potential target for the treatment of type 2 diabetes mellitus [20].

Sirtuin-6 or Mono-ADP ribosyltransferase-sirtuin-6 (SIRT6) is a stress responsive protein deacetylase, and mono-ADP ribosyl transferase enzyme encoded by the SIRT6 gene. Its function in multiple molecular pathways are related to aging, including DNA repair, telomere maintenance, glycolysis, and glucose metabolism and β -cell normal viability. SIRT6 has been shown to play a critical role as the principal regulator of glucose homeostasis. It participates in the expression of gluconeogenesis genes, specifically in the liver [21]. The absence of SIRT6 enzyme has been attributed to increased blood glucose levels therefore, pharmacological modulation of SIRT6 has been the target of several compounds directly relating as a future treatment of type 2 diabetes mellitus [21,22].

On the other hand, the conventional methods of discovering drugs from natural products, such as extraction, qualitative and quantitative identification, are risky and time-consuming processes, the *in silico* approach, comprised of computational methods, facilitates the drug development process by making the analysis efficient [23]. Molecular docking is one of the most extensively employed *in silico* method. This technique is designed to predict the potential of an active molecule in the form of a ligand to form a stable complex with a target protein, usually a receptor [24]. This study investigated

the binding affinities of *Annona muricata* leaf constituents and derivatives towards selected proteins related to Type 2 diabetes mellitus through *in silico* methods.

Methodology

Preparation of Protein Receptors

Two models of 11 β -HSD1, PTP1B and SIRT6 were taken from Research Collaboratory for Structural Bioinformatics (RCSB) protein data bank (PDB) and AlphaFold Protein Structure Database. The PDB models were as follows: 11 β -HSD1 (PDB code: 2BEL), PTP1B (PDB code: 2CM8) and SIRT6 (PDB code: 6QCD) while the protein structures of AF2 models were predicted using DeepMind's Colab notebook [25,26].

The .pdb files of each protein model were processed using AutoDock Tools 1.5.7., water molecules and unwanted atoms were removed, hydrogens were added, and the nonpolar ones were merged. Kollman charges as electrostatic force were also added. Missing residues of the PDB models were assessed and built using SWISS-MODEL and builder's tool of PyMol (for educational use only) [27-29].

Preparation of Ligands

The 3D structures of the 36 parent compounds from the leaves of *Annona muricata* listed in Table 1 were obtained from PubChem server. Each ligand was cleaned in 3D, prepared, and minimized using MMFF94 force field of MarvinSketch 15.6.29. The resulting .mol files were converted to .mol2 file format using OpenBabelGUI v.3.1.1 and further processed using AutoDock Tools 1.5.7. Non-polar hydrogen atoms were merged, Gasteiger partial charges were added to the ligand atoms, and the torsion count or rotatable bonds were checked with the default settings of AutoDock Tools 1.5.7. The resulting files were saved in .pdbqt format and were subjected to molecular docking simulations [27,30-34].

Molecular Docking

AutoDock Vina was utilized for binding affinity measurement through molecular docking [33]. Grid-box optimization was done by redocking the co-crystallized ligands to the empty active binding site of PDB models while the detection of binding pockets of AF2 models were predicted using Discovery Studio Visualizer [34].

The ligands were treated as flexible, while the protein models were set to be rigid. In general, by default, the number of modes was set to 9, 3 kcal/mol for the energy range, and 8 for the exhaustiveness.

Table 1. Average binding energies of the parent compounds towards the six protein models

| Family | Ligand | Average Binding Energy (kcal/mol) | | | | | |
|------------------------|----------------------------------|-----------------------------------|--------------------|-------|------|-------|------|
| | | 11 β -HSD1 | | PTP1B | | SIRT6 | |
| | | PDB | AF2 | PDB | AF2 | PDB | AF2 |
| | | Native ligand ^a | | | | | |
| | Substrate | -12.1 | -8.3 | -9.7 | -6.5 | -7.2 | -9.3 |
| | | -10.5 ^b | -10.5 ^b | - | - | - | - |
| | | -10.1 ^c | -10.3 ^c | - | - | - | - |
| Alkaloids | Annonamine (DAME) | -8.0 | -8.8 | -6.2 | -7.3 | -6.1 | -7.1 |
| | Anonaine (DANE) | -8.2 | -9.3 | -6.6 | -7.7 | -6.6 | -7.7 |
| | Coreximine (DCXE) | -9.1 | -9.1 | -7.0 | -7.1 | -6.5 | -8.2 |
| | Isolaureline (DILE) | -8.1 | -9.6 | -7.1 | -7.6 | -7.0 | -8.1 |
| | Reticuline (DRTE) | -8.8 | -8.6 | -6.6 | -7.0 | -6.7 | -7.4 |
| | Xylopine (DXLE) | -8.5 | -9.0 | -6.6 | -7.8 | -6.7 | -7.4 |
| | Acetogenins | Annonacatalin (GACN) | -7.0 | -8.3 | -5.9 | -6.2 | -5.6 |
| Annomuricin A (GAMA) | | -7.2 | -8.3 | -5.4 | -6.2 | -5.6 | -7.8 |
| Annomuricin B (GAMB) | | -6.9 | -8.7 | -5.5 | -6.3 | -5.6 | -7.7 |
| Annomuricin C (GAMC) | | -7.1 | -8.7 | -5.4 | -6.3 | -5.5 | -7.8 |
| Annomuricin E (GAME) | | -6.9 | -8.6 | -5.6 | -6.3 | -5.6 | -7.9 |
| Annomutacin (GAMT) | | -7.0 | -8.3 | -5.7 | -6.1 | -5.7 | -7.5 |
| Annonacin A (GANA) | | -7.1 | -8.5 | -5.4 | -6.2 | -5.6 | -8.0 |
| Annopentocin A (GAPA) | | -6.9 | -8.3 | -5.8 | -6.2 | -5.8 | -8.0 |
| Annopentocin B (GAPB) | | -6.9 | -8.3 | -5.7 | -6.1 | -5.7 | -8.1 |
| Annopentocin C (GAPC) | | -6.8 | -8.3 | -5.8 | -6.1 | -5.7 | -8.2 |
| Cis-corossolone (GCCS) | | -7.1 | -8.2 | -5.4 | -6.1 | -5.5 | -7.7 |
| Gigantetronenin (GGTN) | | -7.1 | -8.4 | -5.5 | -6.1 | -5.6 | -7.5 |
| Murihexocin (GMHN) | | -6.9 | -8.6 | -6.0 | -6.2 | -5.7 | -8.0 |
| Muricapentocin (GMPT) | | -6.9 | -8.5 | -5.4 | -6.4 | -5.5 | -7.9 |
| Muricoreacin (GMRN) | | -6.9 | -8.6 | -5.9 | -5.6 | -5.6 | -8.0 |
| Muricatocin A (GMTA) | | -6.9 | -8.3 | -5.5 | -6.4 | -5.7 | -7.9 |
| Muricatocin B (GMTB) | | -6.9 | -8.4 | -5.6 | -6.2 | -5.7 | -7.7 |
| Muricatocin C (GMTC) | -6.9 | -8.5 | -5.7 | -6.2 | -5.7 | -7.7 | |
| Phenolic compounds | Chlorogenic Acid (PCAD) | -8.6 | -8.3 | -7.1 | -7.5 | -6.4 | -8.8 |
| | Catechin (PCTN) | -8.8 | -8.8 | -6.5 | -6.7 | -7.7 | -9.7 |
| | Epicatechin (PECE) | -9.0 | -8.7 | -7.7 | -6.8 | -7.2 | -8.3 |
| | Gallic Acid (PGLA) | -6.3 | -6.2 | -5.8 | -5.2 | -5.6 | -6.9 |
| | Kaempferol (PKFL) | -8.4 | -8.7 | -7.7 | -7.1 | -6.8 | -8.3 |
| | Kaempferol 3-O-rutinoside (PKOR) | -9.7 | -10.6 | -7.1 | -9.0 | -6.4 | -7.8 |
| | Quercetin (PQTN) | -8.7 | -9.0 | -8.2 | -7.4 | -7.2 | -8.5 |
| | Rutin (PRTN) | -9.9 | -11.0 | -7.4 | -7.6 | -6.2 | -9.1 |
| Other compounds | Epiloliolide (RELE) | -7.5 | -7.0 | -5.4 | -5.7 | -5.4 | -5.9 |
| | Loliolide (RLLE) | -7.3 | -6.8 | -5.2 | -5.7 | -5.5 | -6.2 |
| | Roseoside (RRSE) | -8.4 | -9.2 | -5.8 | -6.8 | -5.9 | -7.7 |
| | Vomifoliol (RVFL) | -6.5 | -6.8 | -5.3 | -5.8 | -5.5 | -6.5 |

^a Bound ligands for PDB models; CBO (11 β -HSD1), F16 (PTP1B)-Control, QUE (SIRT6)-Control

^b Substrate; Cortisone (11 β -HSD1)-Control

^c Product; Cortisol (11 β -HSD1)

Interaction Analysis

After the initial docking simulation of the *Annona muricata* phytoconstituents, the protein-ligand complex of the 36 parent compounds was saved in .pdb format using PyMol (education-use-only) and used as the input file in LigPlot Plus. All the interacting residues and types of interaction present were listed and analyzed [29,36].

Generation of Derivatives

The generation of derivatives was done by selecting the topmost active parent compounds. They were subjected to single and combined modifications, and metabolite prediction.

Bioisosteric Replacement

For single modifications, the generated molecular replacements by MolOpt and SwissBioisostere were considered based on the synthetic accessibility scores of the resulting analogues [37,38]. Identification and assessment of the points of molecular substructural replacements were made after initial molecular docking simulation of the topmost parent compounds. After single modifications, multisite variations were performed. This was done by selecting the best functional group per point of replacement of each parent compound based on their affinity scores in all protein targets.

The modifications of the 3D structures of all the analogues were processed using MarvinSketch 15.6.29 and were prepared the same way as the parent compounds and subjected to molecular docking.

Metabolite Prediction

Phase I (CYP 450) biotransformation was selected for the prediction of the primary metabolites. The .sdf files of the active compounds were submitted to SMARTCyp, an online web tool used to predict the most liable moieties to cytochrome P450 mediated metabolism. Furthermore, MetaTox and Biotransformer3.0, all open-access web service tools, were also used for *in silico* metabolite prediction [39-41].

ADMET and Physicochemical Analysis

The derivatives and their corresponding parent compounds, that exhibited more negative binding energies than controls for each protein target were subjected to pharmacokinetic and physicochemical assessment. The different properties used to evaluate the compounds were grouped into major categories and can be seen Appendix A. All these parameters were evaluated using SwissADME and ADMETlab 2.0. The SMILES of the ligands were used as input values and the CSV outputs were downloaded, listed and evaluated [42,43].

Data Analysis

The average binding free energy of the top and lowest values generated from molecular docking was recorded and evaluated. All the interacting residues, the numbers and types of bonds, including hydrogen bonding and hydrophobic interactions were assessed.

Results

Grid box optimization

The appropriateness of grid box parameters is determined by calculating the root-mean-square distance (RMSD) of the redocked conformations relative to the original pose of the co-crystallized ligand. Additionally, the RMSD between matching atom pairs is also used to measure the degree of similarity between two three-dimensional (3D) protein structures [44]. For an accurate prediction of the bound conformation and structural similarity of biological structures, the RMSD should be less than or equal (\leq) to 2Å [34], or the smaller the RMSD, the more similar the two structures [45].

The results of grid box optimization are shown in Appendix B. These were then used as grid box parameters for the 36 ligands for each PDB model of the protein targets. For the AF2 models, the values of binding attributes of site one provided by Discovery Studio Visualizer were considered as this covers the reported significant residues of each protein target. The reported amino acid residues listed in Appendix C were checked and matched in both PDB and AF2 models.

The grid box and docking parameters were considered valid by ensuring that the average RMSD relative to the original pose is less than 2Å as shown in Appendix D. 2BEL model of 11β-HSD1 has an average RMSD of $0.819 \pm 0.003\text{Å}$, 2CM8 model of PTP1B has an average RMSD of $0.335 \pm 0.001\text{Å}$, and 6QCD model of SIRT6 has an average RMSD of $1.733 \pm 0.010\text{Å}$. On the other hand, the RMSD of the superimposed PDB (blue) and AF2 (yellow) models of 11β-HSD1, PTP1B and SIRT6 target, are 1.169Å, 0.687Å, and 1.033Å, respectively.

Binding energies

After successfully identifying the grid box parameters, the 36 constituents of *Annona muricata* leaves were subjected to molecular docking. The average top binding energy of each protein-ligand pair can be seen in Table 1. It can be observed that the binding energies of the 36 ligands range from of -5.2 to -11.0 kcal/mol. Compared to controls, PRTN and PKOR exhibited the lowest binding energies in AF2 models of 11β-HSD1 and PTP1B, respectively. In SIRT6, PCTN showed the lowest binding energy on both PDB and AF2 models.

For easier comparison, the mean of the binding energies of each ligand towards the PDB and AF2 models of each protein target were calculated. The mean energy scores are generally lower in 11β-HSD1 compared to the other two targets. It is followed by SIRT6, except for DAME, DXLE and PKOR, which exhibited lower average scores in PTP1B. Another noticeable ligand is DANE, which exhibited an equal mean energy with SIRT6 and PTP1B. The rest of the parent compounds bound to PTP1B with mean binding energies have less affinity than SIRT6. This can be found in Appendix E.

Single modifications

After initial docking simulations of the parent compounds, the 36 ligands of *Annona muricata* were filtered to identify the active ligands in all models which were then considered for drug design. The analysis was done by applying a 2.85 kcal/mol threshold based on standard error of AutoDock Vina, getting the difference

between the binding energies of the ligands and the controls. As a result, the 8 parent compounds – the alkaloids DCXE and DILE, and phenolic compounds PCAD, PECE, PKFL, PKOR, PQTN, and PRTN were selected and subjected to bioisosteric modifications.

The suggested bioisosteres by MolOpt and SwissBioistere were considered and used in each point of replacement (R). By altering the R groups that were present in the basic framework of each parent compound, a total of 305 single structurally modified analogues were designed and tested against the selected protein targets.

Combined modifications

The combined modifications were developed using the best bioisosteres and the selection of final points of replacement for the 8 selected parent compounds. This was done by comparing the average binding energies of each single structurally modified analogue across all targets with their corresponding parent compound. For a bioisostere to be considered, an analogue's binding energy must be less than or equal (\leq) to the average binding energy of the parent compound. By generating all the possible combinations for each parent compound, a total of 297 structural analogues were designed.

Metabolite prediction

Using the top 8 parent compounds as framework, and the designation of the potential sites of metabolism (SOMs) and possible metabolites, a total of 70 phase 1 biotransformation products were predicted, designed and tested against the protein targets.

Docking results

A total of 672 derivatives composed of structural analogues and predicted metabolites were generated and subjected to molecular docking. Out of these 672 derivatives, 280 derivatives, all of which are structural analogues, exhibited mean binding energies which are less than or equal (\leq) to the mean binding energy of the control for at least one of the three protein targets. Of these 280 potential derivatives, 137, 155, and 121 compounds have shown improved binding energies than the controls for 11 β -HSD1, PTP1B, and SIRT6, respectively.

In terms of individual targeting, these structural analogues were consolidated and ranked based on their binding energies to identify the top derivatives for each protein target. The structures of the top 5 derivatives for 11 β -HSD1, PTP1B and SIRT6 are illustrated in Figure 1.

Compounds ACM021, ACM036, ACM044, ACM018, and ACM024, all of which are derivatives of PRTN are the top 5 derivatives for 11 β -HSD1. In PTP1B, ACM014, ACM021, ACM028, ACM020, and ACM024, also derivatives of PRTN, are the top 5 ligands. Lastly, BCM008, DCM027, DCM004, DCM025, and BCM022 the top 5 derivatives for SIRT6; the 2nd to 4th compounds are derivatives of PECE while the other two are derived from PKOR.

Interaction analysis

All 36 *Annona muricata* parent compounds together with the known substrates and co-crystallized ligands were subjected to interaction analysis with the 3 protein targets. Since every protein target has two models, PDB and AF2, identification was done per model and summarized to show the types of interactions present, and the interacting residues involved. The summary of the identified interacting amino acid residues and types of interactions are shown in Figure 2 and Figure 3.

The interacting residues were further analyzed to identify the top active residues that tend to possess a high affinity and selective binding to each protein target. The types of interactions were also categorized into hydrogen or hydrophobic bonds.

In Figure 2A, out of 78 (cumulative) ligands in 11 β -HSD1, Ser170 and Tyr183 exhibited the most number of interactions, with 76 and 75 interacting ligands in both models, respectively. As for the type of interactions, Ser170 exhibited the greatest number of hydrogen bonding with all the docked ligands having a total of 43, while Ala223 exhibited the greatest number of hydrophobic bonding with a total of 49 interacting ligands as shown in Figure 3A.

In PTP1B (Figure 2B), among the listed amino acid residues, out of 74 (cumulative) ligands, Tyr046, Phe182 and Ala217 are most active residues as they show the most number interactions with all docked ligands. On the other hand, as shown in Figure 3B, Asp048 exhibited the most number of hydrogen bond interactions, specifically to interact with 37 ligands while Phe182 for hydrophobic interactions with 49 interacting ligands.

Among the identified amino acid residues in SIRT6 (Figure 2C), all 74 (cumulative) ligands exhibited an interaction with the reported amino acid residue Phe064 hence, considered as the most active residue. However, for the types of interactions, the unreported amino acid residues Arg065 and Ile219 exhibited the most significant number of hydrogen and

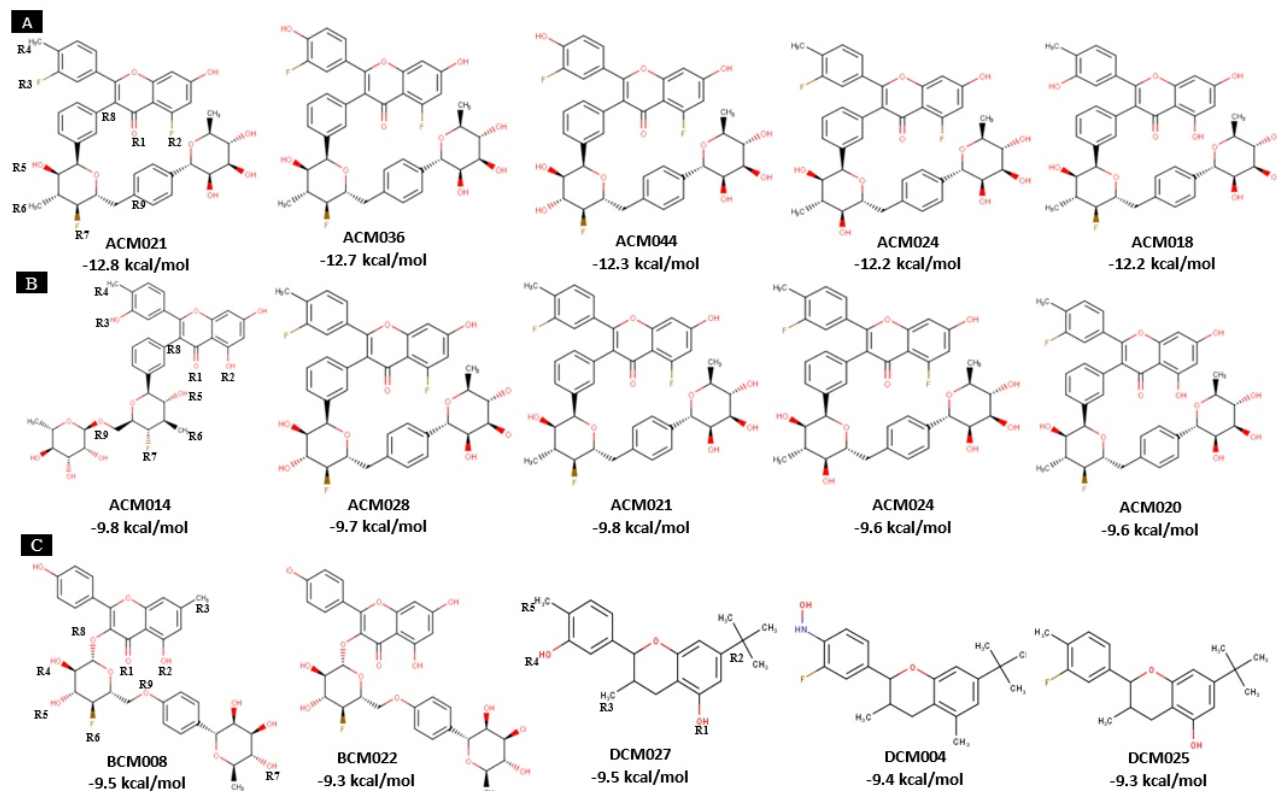


Figure 1. Two-dimensional structures and binding energies of the top 5 derivatives. A:11β-HSD1, B:PTP1B, C: SIRT6

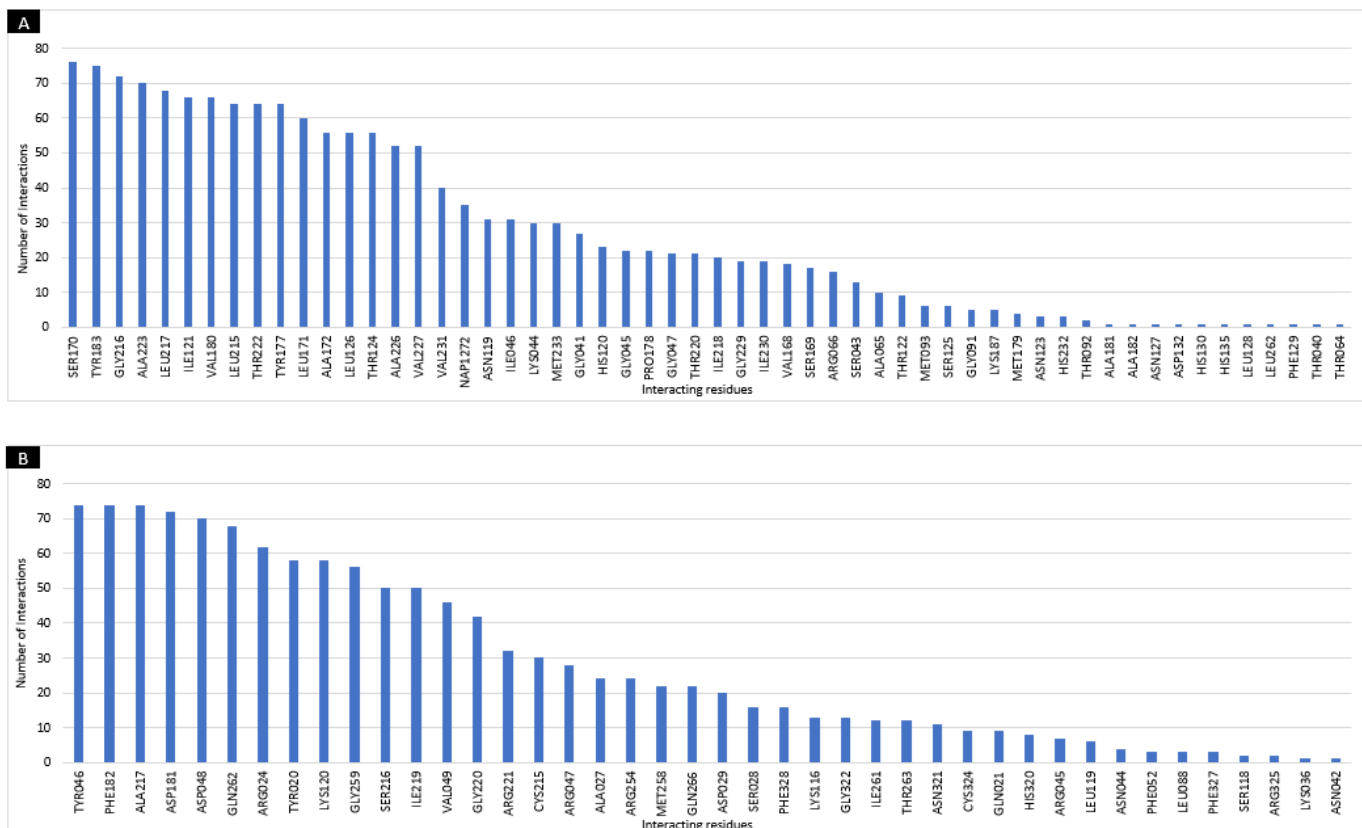


Figure 2. Summary of the interacting amino acid residues in all protein targets. A:11β-HSD1, B:PTP1B, C:SIRT6

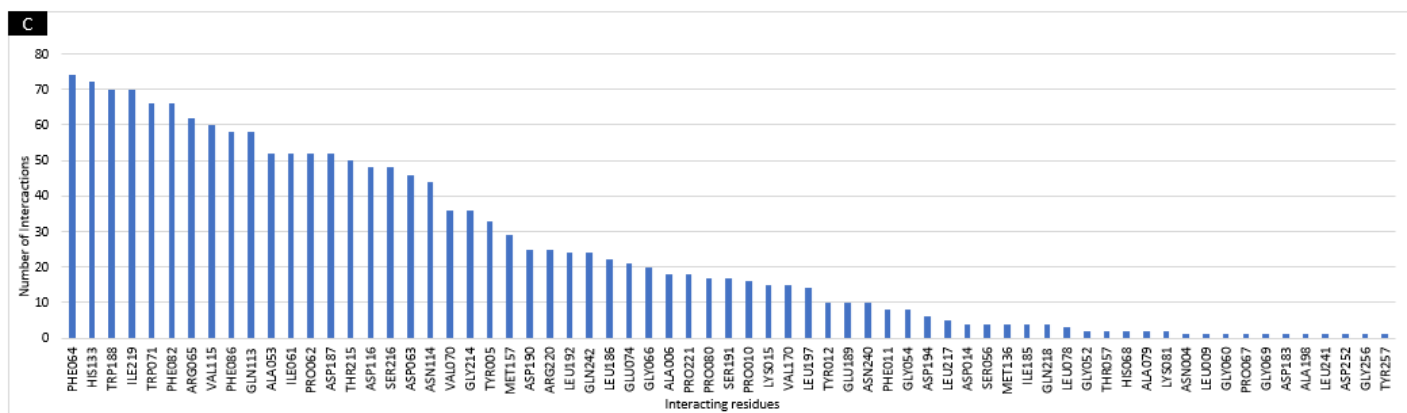


Figure 2. (Continuation)

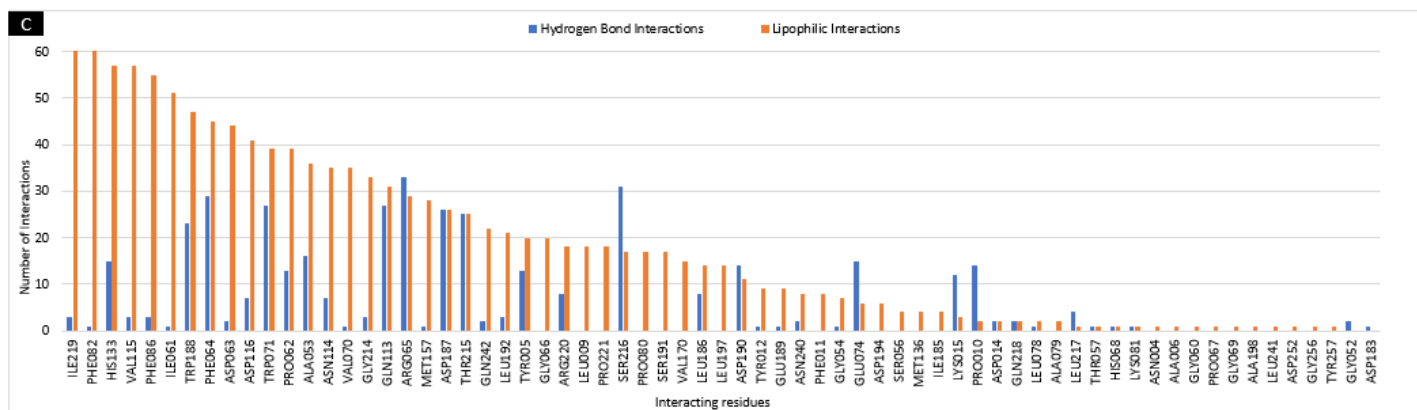
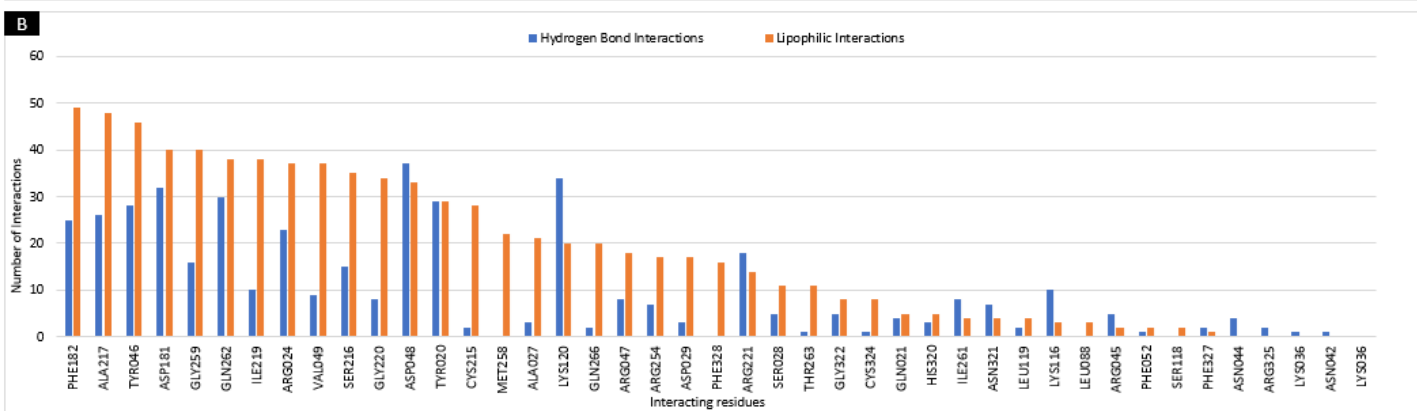
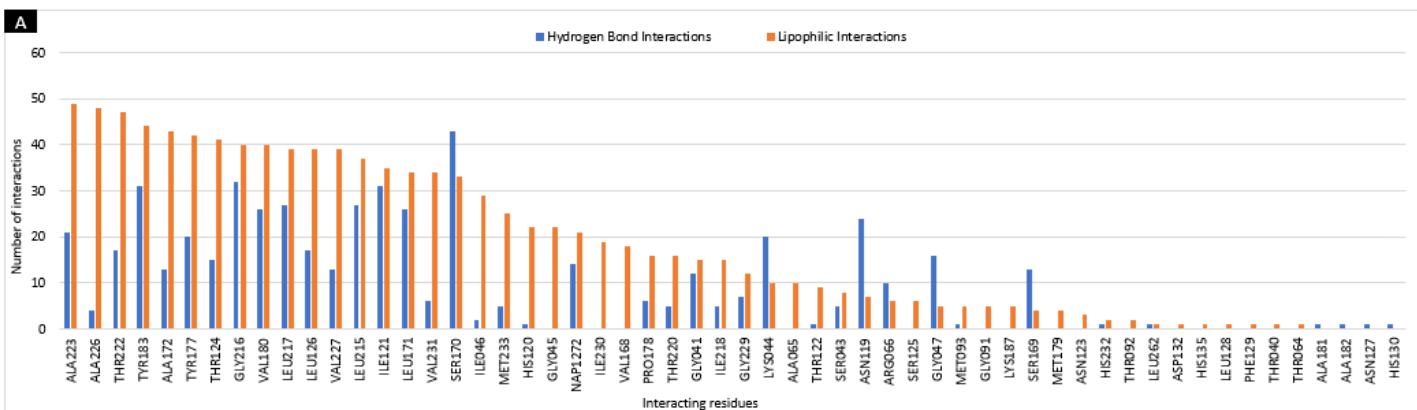


Figure 3. Summary of interactions in all protein targets. A:11β-HSD1, B:PTP1B, C:SIRT6

hydrophobic bonding interactions having 33 and 67 interacting ligands, respectively (Figure 3C). Moreover, Gly111, and Thr213 were reported in previous studies but did not show any interactions in any of the parent compounds.

ADMET and Physicochemical Analysis

All the 280 potential derivatives and their corresponding parent compounds were subjected to ADMET and physicochemical analysis. This analysis was done as an additional characterization of the designed analogues and their corresponding parent compounds. The criteria for evaluating whether a compound is said to fulfill a certain property was based on its acceptability in all of the parameters.

Figure 4 shows that in 11 β -HSD1, 2.8% or 4 compounds passed all of the absorption parameters. These fully absorbed compounds were mostly from DILE and PKFL. For distribution parameters, PRTN and PKOR derived analogues comprised of 17.7% or 25 compounds passed all the conditions. The same group of analogues passed the metabolism with 46.1%, or 65 compounds. DILE derived compounds comprised of 2.8% or 4 compounds passed the excretion while 68.1% or 96 compounds from PRTN and PKOR analogues passed the toxicity screening. PRTN derived analogues with 4.3% or 6 compounds met the ideal physicochemical properties. Lastly, DILE analogues with 5% or 5 compounds were predicted to be drug-like molecules.

In PTP1B, most of the PQTN and DILE derived compounds passed all absorption screens with 14.9%, or 25 compounds. PRTN and PKOR derivatives with 14.3% or 24 compounds have the ideal distribution profiles. The same groups with 68 compounds or 42.2% were also predicted as inactive substrates and inhibitors of the major CYP450 isozymes. All the 3.1%, or 5 compounds, are DILE analogues that were predicted to be well excreted. The non-toxic 60.9%, or 98 compounds, were from PRTN and PKOR. The derived compounds of PRTN, PKFL, PCAD, and PQTN with 12.4% or 20 compounds met the ideal physicochemical properties. On the other hand, 6.2% or 10 compounds that were predicted to be drug-like molecules are PQTN and DILE derived compounds.

Moreover, in SIRT6, 47.3% or 61 compounds passed all of the absorption parameters. These derivatives are analogues of PQTN, PECE, DILE, PKFL, and DCXE. Most PRTN, PKOR, and PCAD analogues comprising 7.1%, or 22 compounds, passed the distribution. The same group of derived compounds with 20.9% or 27 compounds passed the metabolism, 26.4% or 34 compounds passed the excretion, majority from PECE. The derive compounds of PRTN, PKOR, PQTN, and PECE with

79.1% or 102 compounds passed the toxicity screening. Most PECE analogues comprising 33.3%, or 43 compounds, possessed the ideal physicochemical properties, and 63.6%, or 82 compounds from PQTN and PECE were predicted as drug-like molecules.

Lastly, for synthetic accessibility, all the designed analogues and their corresponding parent structures in all targets met the criteria of being synthetically accessible.

The data in Figure 4 were further processed to identify the best ligand in each protein target that fulfills the most number of properties. The properties of these ligands can be found in Appendix F and illustrated in Appendix G. ASM021, a derivative of PRTN exhibited -10.8 kcal/mol, had the most number of passed ADMET and physicochemical screens and considered the best ligand for 11 β -HSD1. HCM004, a compound derived from PCAD exhibited -8.2 kcal/mol for PTP1B, and the PECE-derived compound, DSM008 for SIRT6 exhibited -8.3 kcal/mol.

Discussion

Grid Box Optimization

As shown Appendix D, with the RMSD values, all of which are less than 2 Å , the comparison of the models and the grid box used in redocking were considered structurally similar and valid. The grid boxes were then used for all molecular docking simulations of the parent compounds and derivatives. They were assessed primarily based on their binding energies (kcal/mol).

Binding Towards 11 β -HSD1

Several studies have been conducted for the potential inhibitors of 11 β -HSD1 [17,55]. Carbenoxolone, a glycyrrhetic acid derivative, was the first 11 β -HSD1 inhibitor tested in humans. Even though it is not selective, it has demonstrated the ability to increase insulin sensitivity [56]. Gossypol, a polyphenol toxin produced from cotton plant seeds and root skin, suppressed 11 β -HSD1 activity in the rat liver and human adrenal gland, indicating that it may be utilized as an inhibitor, although it was later discovered to be a non-selective inhibitor [57].

The focus of this study is to find potential candidates that can competitively inhibit the binding of cortisone to the catalytic site of 11 β -HSD1, to potentially arrest the action of the enzyme in converting cortisone to cortisol hence, cortisone was used as a control for screening the experimental ligands.

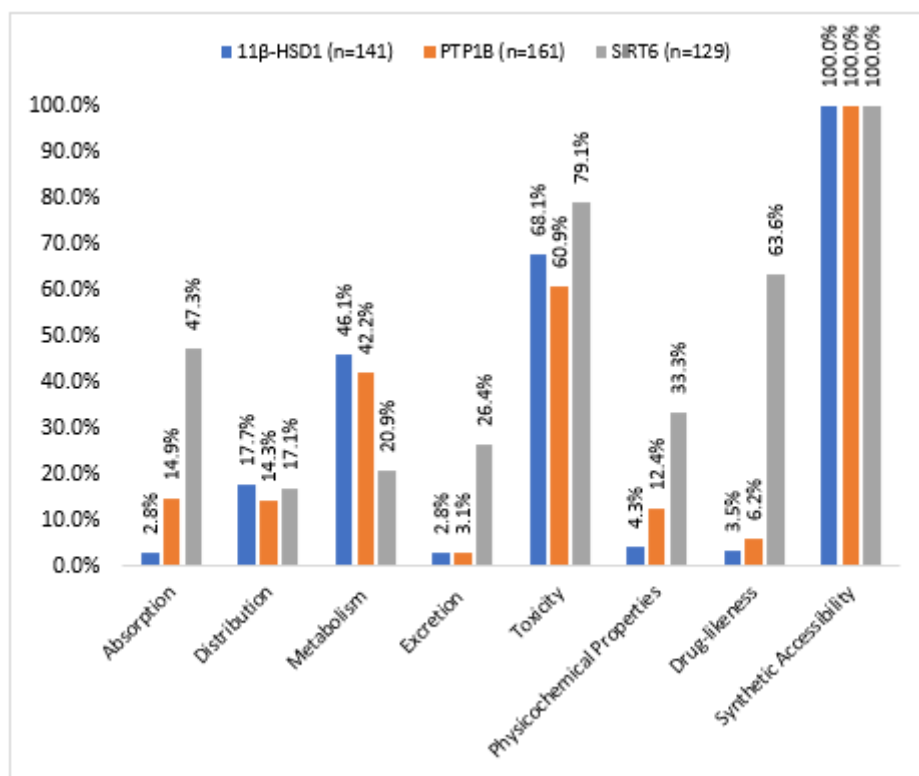


Figure 4. Evaluation of the 280 potential derivatives for each protein target based on ADMET-physicochemical properties

Based on the average values of the binding free energy listed in Table 1, it is evident that the redocked CBO exhibited the lowest binding energy, having -12.1 kcal/mol in the PDB model, but generating -8.3 kcal/mol in the AF2 model. In terms of the AF2, it can be observed that out of the 36 ligands, specifically in comparison with cortisone as the control, only PRTN and PKOR exhibited more negative binding energies having -11.0 and -10.6 kcal/mol, respectively. On the contrary, PGLA has the least binding energy for PDB and AF2 models of 11β-HSD1 having -6.3 kcal/mol and -6.2 kcal/mol, respectively.

As for the average binding energies of parent compounds in both models of 11β-HSD1, PRTN has an equal binding energy with the cortisone (-10.5 kcal/mol), and lower binding energy than CBO (-10.2 kcal/mol). Considering the ±2.85 kcal/mol threshold as the standard error of AutoDock Vina, most of the parent compounds fall within the acceptable range of having a comparable binding affinity with cortisone.

The amino acid residues of 11β-HSD1 listed in Appendix C were found to be essential for its catalytic reaction [46-48]. Ser170 and Tyr183 have been considered as the most crucial interacting residues for catalysis when it comes to the reduction of cortisone to cortisol, as these 2 residues form the close contact with C-11 hydroxyl of the cortisol. These

two residues increase the electrophilicity of the reactive C-11 atom of cortisone, thereby facilitating the proton transfer from Tyr183, which is reduced by electrostatic interactions with the substrate 11-keto oxygen and thus converting cortisol to its active form [45]. These reported residues have also been observed after molecular docking simulations of the parent compounds to the catalytic site of 11β-HSD1 enzyme. As shown in Figure 2A, Ser170 and Tyr183 are the most active residues. Ala223 and Ser170 had the most number of hydrophobic and hydrogen bond interactions in both models. These residues reflect their critical roles in the catalytic activity of 11β-HSD1 as they were found to exhibit most number of the interactions with docked ligands.

Based on the top 5 structural analogues for 11β-HSD1 Figure 1A, the presence of phenyl ring as a replacement to R8 and R9 ether linkers, R2, R3, and R7 hydroxyls replaced by a fluoro substituent, and the R4 and R6 hydroxyls substituted by methyl improved the binding energies towards 11β-HSD1.

Binding Towards PTP1B

Insulin receptor desensitization is one of the primary functions of Protein Tyrosine Phosphatase 1B (PTP1B). Since inhibition of this enzyme may prolong the activity of insulin receptors, PTP1B has emerged as a potential therapeutic

target for type 2 diabetes [20]. Vanadium containing compounds were investigated as PTP1B inhibitors. However, randomized clinical trials for the treatment of diabetes concluded that these drugs caused GI distress, showed low efficacy among diabetic patients, and showed large patient-to-patient variability [58]. Triaryl-sulfonamides were reported to form hydrogen bonding interactions with critical residues of PTP1B [59]. However, these potential compounds faced the limitation of poor cell membrane permeability [60].

After the docking simulation of the parent compounds in PTP1B, none of the 36 ligands outperformed the binding energy of the bound control in the PDB model. In contrast to this, some parent compounds showed lower binding energies with control in AF2 model including PRTN and PKOR as the top parent compounds. RLLC and PGLA generated the least binding energy having both -5.2 kcal/mol. Based on the average binding energies of parent compounds in both models and applying the ± 2.85 kcal/mol as the standard error, all of the parent compounds fall within the acceptable range of having a comparable binding affinity.

The active site of PTP1B consists of the amino acid residues His214–Arg221, which contain the catalytic site nucleophiles Cys215 and Arg221. Tyr046, Val049, Lys120, Asp181, Phe182, and Gln262 are additional residues that form the sides of the catalytic cleft and contribute to catalysis and substrate recognition [49-51]. These reported essential amino acid residues were all recorded to have interactions with the docked ligands. Moreover, as shown in Figure 2B, Tyr046, Phe182 and Ala217 were found to be the most active residues to interact with all of the docked ligands. On the other hand, Asp048 and Phe182 has the greatest number of interactions in all ligands in both PDB and AF2 models.

In PTP1B, as shown in Figure 1B, these explain that the substitution of phenyl ring as the ether linker groups, replacement of fluoro substituent in the R2, R3, and, R7 hydroxyl groups, placement of methyl substituent at R4, and R6 hydroxyls, and the retention of original substituents such as the carbonyl and hydroxyl group at R1, and R5 positions improved the binding affinities towards PTP1B enzyme.

Binding Towards SIRT6

Sirtuin-6 or Mono-ADP ribosyltransferase-sirtuin-6, although it is associated with physiological and pathological processes, it has also been recognized to have a vital role in the metabolism of glucose. Several studies have proven that the elimination of SIRT6 from the entire body resulted in severe hypoglycemia in mice. Its absence is associated with hepatic

steatosis and insulin resistance. Moreover, its activation also provides protection against obesity and diabetes [51]. The flavonoids luteolin and quercetin were also evaluated as SIRT6 modulators and demonstrated a dose-dependent role, whereby they exert inhibitory activity at low concentrations and modulatory activity at high concentrations [54].

As a result of docking analysis, since quercetin served as the control for SIRT6 enzyme and one of the parent compounds is quercetin as well, they generated the same binding energies for PDB model having -7.2 kcal/mol. However, in AF2 model, PQTN as experimental ligand yielded a lower binding energy than the control having -8.5 kcal/mol. On the other hand, aside from PQTN, PECE also shows the same binding energy as compared to control in PDB model. PCTN has -7.7 kcal/mol and -9.7 kcal/mol being both showed a better binding energy in both models. These docking results support the study proving that quercetin and its based compounds catechin and epicatechin have good binding profiles and biological effects against SIRT6 [52].

In contrast, RELE has the least binding energy for both PDB and AF2 models, having -5.4 kcal/mol and -5.9 kcal/mol, respectively. As for the average binding energies of parent compounds in both models of SIRT6 and applying the 2.85 kcal/mol as the standard error, all of the parent compounds fall within the acceptable range of having a comparable binding affinity having PQTN and PCTN as the top compounds.

SIRT6 enzyme has been implicated in several biological processes including glucose homeostasis regulated by beta cells, its extended acyl binding channel confirm its specificity among other isoforms. Reported amino acid residues in the binding site region has also been documented to play roles in SIRT6 functions [53,54]. The reported amino acid Phe064 was considered to be the most active residue to interact with the docked ligands in both PDB and AF2 models. This reflects that Phe064 is the most crucial amino acid residue in SIRT6. In contrast to this, the additional interacting residues Ile219 and Arg065 were observed to have the most number of hydrophobic and hydrogen bond interactions in both models hence, can be added as significant residues for SIRT6 functions.

Based on the top 5 compounds in SIRT6 as shown in Figure 1C, BCM008 and BCM022 as PKOR derivatives, along with PECE-derived compounds DCM004, DCM027, and DCM025, were the best ligands to have the highest binding affinity towards the SIRT6 target. These explain that the attachment of phenyl ring in the R8 ether linker, replacement of fluoro substituent in R6 hydroxyl, and methyl group in the R3 hydroxyl of PKOR improved their binding energies. Also, the binding

energies improved in PECE analogues with methylpropane and a methyl group at R2 and R3 hydroxyls, methyl, -NHOH, or a fluoro substituent at R4 hydroxyls.

ADMET and Physicochemical Predictions

In pharmacokinetic and physicochemical screening, various parameters of absorption, distribution, metabolism, excretion, toxicology (ADMET), and drug-like properties were considered.

As for the best candidate for each protein target, for ASM021 in 11 β -HSD1, minimal consideration for some modifications in dosing and contraindications might improve the excretion and absorption parameters. Except for having poor absorption and excretion profiles, ASM021 was predicted to be a well distributed, inactive substrate and inhibitor of the CYP450 isozymes, non-toxic, and has an acceptable solubility profile.

In PTP1B, out of 155 analogues, HCM004, a compound derived from PCAD, fulfills the most number of ADMET and physicochemical filters. HCM004 was predicted to have ideal distribution, metabolism, toxicity, drug-likeness, and physicochemical profiles. However, HCM004 was predicted to have an increased property of being a P-gp substrate.

Lastly, for SIRT6, the PECE-derived compound, DSM008, had the most accepted profiles out of the 121 analogues. Except for having a short half-life, DSM008 was predicted to be a well-absorbed, distributed, inactive inhibitor and substrate of the major CYP450 isozymes, non-toxic, a drug-like molecule, and has the ideal solubility profile, it also decreased the property of being an active CYP2C9 substrate and a compound with a low therapeutic index.

In summary, *in silico* methods were utilized in this study for the preliminary screening of the selected phytoconstituents of *A. muricata* and derivatives for potential binding with the protein targets related to T2DM: 11 β -HSD1, PTP1B, and SIRT6. Based on the binding energies of the parent compounds and derivatives, their differences still fall within the ± 2.85 kcal/mol standard error of AutoDock Vina hence a significant difference cannot be claimed. This means that those parent compounds and derivatives have comparable binding affinity as the controls. Out of 280 potential derivatives, 137, 155, and 121 compounds have shown improved binding energies than the controls for 11 β -HSD1, PTP1B, and SIRT6, respectively. Moreover, none of the metabolites have exhibited better binding than controls.

Structural modifications of the basic framework of the parent compounds were also noticed to improve the

binding scores of some analogues than the controls hence, were considered as potential derivatives.

Interaction analysis reveals that most of the reported binding residues have been observed to interact with most of the experimental ligands. As indicated by the presence of aromatic compounds, most of the observed interactions were hydrophobic. The most active residues in 11 β -HSD1 are Ser170 and Ala223, both of which can form hydrogen and hydrophobic bond interactions. On the other hand, the most active PTP1B residues involved in hydrogen bond and hydrophobic interactions are Asp048 and Phe182. Lastly, Arg065 and Ile219 exhibited the significant number of hydrogen and hydrophobic bond interactions in SIRT6.

Pharmacokinetic and physicochemical analysis have shown that some modifications were found to improve the pharmacokinetic properties of the parent compounds, such as in the case of ASM021 which had increased lipophilicity and human intestinal absorption rate. Another example is HCM004. While it became a full substrate of P-gp, its lipophilicity did improve and its capability to induce CNS effects was reduced when compared to PCAD. Lastly, relative to parent compound, DSM008 showed improved plasma protein binding (PPB) and evasion against CYP2C9 metabolism. In relation on the pharmacokinetic and physicochemical analysis, this improvements in the designed derivatives demonstrated favorable druggability, as they showed more negative binding energies hence, more stable affinity to the active binding sites of the protein targets.

Based on these findings, some recommendations can be considered. To fully assess the enzymatic activity of the designed compounds found to have a comparable binding affinity with the target proteins, this study suggests a preparatory drug synthesis, specifically for the top 5 ligands in 11 β -HSD1, PTP1B, and SIRT6, which exhibited the most spontaneous binding with each protein target. And then can be used in performing *in vitro* and *in vivo* experiments to determine their actual biological effects – whether they will serve as inhibitors, activators, or modulators of the target enzymes of interest.

Acknowledgement

The authors would like to thank the Philippine Department of Science and Technology—ASTHRDP for financing this research work.

Author Disclosure

We declare we have no competing interests and/or no financial competing interests, or other interests that might be perceived to influence the interpretation of this article.

References

- Coria-Téllez A, Montalvo-González E, Yahia E, Obledo-Vázquez E. (2016) *Annona muricata*: A comprehensive review on its traditional medicinal uses, phytochemicals phypharmacological activities, mechanisms of action and toxicity. *Arabian Journal of Chemistry*, 11(5), 662–691. doi:10.1016/j.arabjc.2016.01.004
- Vasquez M. (1990) Useful Plants of Amazonian Peru Second Draft. National Agricultural Library (US).
- Adewole S, Caxton-Martins E. (2009) Morphological changes and hypoglycemic effects of *Annona muricata* linn. (Annonaceae) leaf aqueous extract on pancreatic β -cells of streptozotocin-treated diabetic rats. *African J Biomed Res* 9(3):173-187. doi:10.4314/ajbr.v9i3.48903
- Takahashi J, Pereira C, Imenta L, Boaventura M, Silva L. (2006) Antibacterial activity of eight Brazilian Annonaceae plants. *Nat Prod Res*. 2(1):21-6. doi: 10.1080/14786410412331280087.
- Heinrich H, Kuhnt M, Wright C, Rimpler H, Phillipson A, Schandelmaier J, Warhurst D. (1992) Parasitological and Microbiological Evaluation of Mixe Indian Medicinal Plants (Mexico). *Journal of Ethnopharmacology*, 36(1), 81–85. doi:10.1016/0378-8741(92)90063-w
- Boyom F, Fokou P, Yamthe L, Mfopa A, Kemgne E, Mbacham W, et al. (2011) Potent antiplasmodial extracts from Cameroonian Annonaceae. *Journal of Ethnopharmacology*, 134(3):717-724. doi:10.1016/j.jep.2011.01.020
- Moghadamtousi S, Fadaeinasab M, Nikzad S, Mohan G, Ali H, Kadir H. (2016) *Annona muricata* (Annonaceae): A review of its traditional uses, isolated acetogenins and biological activities. *International Journal of Molecular Sciences*, vol. 16, no. 7. MDPI AG, pp. 15625–15658.
- N’Gouemo P, Koudogbo B, Tchivounda H, Akonon-guema C, Etoua, M. (1997). Effects of ethanol extract of *Annona muricata* on pentylenetetrazol-induced convulsive seizures in mice. *Phytotherapy Research*, 11(3), 243–245. doi:10.1002/(sici)1099-1573(199705)11:3<243::aid-ptr66>3.0.co;2-a
- Souza D, dos Santos Sales V, de Souza Rodrigues C, de Oliveira L, Santiago Lemos I, de Araújo Delmondes. et al. (2018) Phytochemical Analysis and Central Effects of *Annona Muricata* Linnaeus: Possible Involvement of the Gabaergic and Monoaminergic Systems. *Iranian Journal of Pharmaceutical Research: IJPR*, 17, 1306-1317.
- Badrie N, Schauss AG. (2009) Soursop (*Annona muricata* L.): composition, nutritional value, medicinal uses, and toxicology. In: *Bioactive Foods in Promoting Health*. 621–643.
- International Diabetes Federation. (2021) *Diabetes Atlas*, 10th ed. <https://diabetesatlas.org/>
- Galicia-Garcia U, Benito-Vicente A, Jebari S, Larrea-Sebal A, Siddiqi H, Uribe K, Martín C. (2020). Pathophysiology of Type 2 Diabetes Mellitus. *International Journal of Molecular Sciences*, 21(17), 6275. doi:10.3390/ijms21176275
- Trang Nguyen N, Le L. (2012) Targeted proteins for diabetes drug design. *Advances in Natural Sciences: Nanoscience and Nanotechnology*, 3(1), 013001. doi:10.1088/2043-6262/3/1/013001
- Henquin JC. (2004) Pathways in Beta-Cell Stimulus-Secretion Coupling as Targets for Therapeutic Insulin Secretagogues. *Diabetes*, 53(Supplement 3), S48-S58. doi:10.2337/diabetes.53.suppl_3.s48
- Gregory S, Hill D, Grey B, Ketelbey W, Miller T, Muniz-Terrera G. et al. (2020) 11 β -Hydroxysteroid Dehydrogenase Type 1 Inhibitor Use in Human Disease—a Systematic Review and Narrative Synthesis. *Metabolism*. 2020;108. doi:10.1016/j.metabol.2020.154246
- Geer B, Islam J, Buettner C. (2014) Mechanisms of Glucocorticoid-Induced Insulin Resistance: Focus on Adipose Tissue Function and Lipid Metabolism. *Endocrinol Metab Clin North Am*. 43(1):75. doi:10.1016/J.ECL.2013.10.005
- Almeida C, Monteiro C, Silvestre S. (2021) Inhibitors of 11 β -hydroxysteroid dehydrogenase type 1 as potential drugs for type 2 diabetes mellitus—a systematic review of clinical and in vivo preclinical studies. *Sci Pharm*. 89(1):1-14. doi:10.3390/scipharm89010005
- Patel H, Dhangar K, Sonawane Y, Surana, S, Karpoormath R, Thapliyal N. et al. (2018) In search of selective 11 β -HSD type 1 inhibitors without nephrotoxicity: An approach to resolve the metabolic syndrome by virtual based screening. *Arabian Journal of Chemistry*, 11(2), 221–232. doi:10.1016/j.arabjc.2015.08.003
- Begum N, Nasir A, Parveen Z, et al. (2021)

- Evaluation of the Hypoglycemic Activity of *Morchella conica* by Targeting Protein Tyrosine Phosphatase 1B. *Front Pharmacol.* 12. doi:10.3389/fphar.2021.661803
20. Zhang S, Zhang ZY. (2007) PTP1B as a drug target: recent developments in PTP1B inhibitor discovery. *Drug Discovery Today.* 12(9-10):373-381. doi:10.1016/j.drudis.2007.03.011
 21. Khan R, Nirzhor S, Akter R. (2018) A Review of the Recent Advances Made with SIRT6 and its Implications on Aging Related Processes, Major Human Diseases, and Possible Therapeutic Targets. *Biomolecules*, 8(3), 44. doi:10.3390/biom8030044
 22. Bae E. (2017) Sirtuin 6, a possible therapeutic target for type 2 diabetes. *Arch Pharm Res.* 40(12):1380-1389. doi:10.1007/s12272-017-0989-8
 23. Andleeb S, Nadia A, Waqar H, Nouman R. (2020) In silico discovery of potential inhibitors against Dipeptidyl Peptidase-4: A major biological target of Type-2 diabetes mellitus, *Int J Clin Microbiol Biochem Technology* 3(1):001-010. doi:10.29328/journal.ijcmbt.1001008
 24. Abirami N, Arulmozhi R. (2017) In-silico approach towards protein targets related to diabetes mellitus - An Overview. *Orient J Chem.* 33(4):1614-1622. doi:10.13005/ojc/330404
 25. Berman H, Westbrook J, Feng Z, Gilliland G, Bhat T, Weissig H, et al. (2000) The Protein Data Bank. 28(1):235-242.
 26. Ronneberger O, Tunyasuvunakool K, Bates R, Židek A, Ballard A, Cowie A, et al. (2021) Nature. 596(August). doi:10.1038/s41586-021-03819-2
 27. Huey R, Morris G, Forli S. (2012) Using AutoDock 4 and AutoDock Vina with AutoDockTools: A Tutorial *Scripps Res Inst Mol.* :32.
 28. Arnold K, Bordoli L, Kopp J, Schwede T. (2006) The SWISS-MODEL workspace: A web-based environment for protein structure homology modelling. *Bioinformatics.* 22(2):195-201. doi:10.1093/bioinformatics/bti770
 29. Schrödinger, L. DeLano W. (2020) PyMOL. <http://www.pymol.org/pymol>.
 30. Damayanti D, Utomo D, Kusuma C. (2017) Revealing the Potency of *Annona Muricata* Leaves Extract as FOXO1 Inhibitor for Diabetes Mellitus Treatment through Computational Study. In *Silico Pharmacology*, vol. 5, no. 1, Springer Science and Business Media LLC. doi:10.1007/s40203-017-0023-3.
 31. Morris G, Huey R, Lindstrom W, Sanner M, Belew R, Goodsell D. et al. (2009) AutoDock4 and AutoDockTools4: Automated docking with selective receptor flexibility. *Journal of Computational Chemistry*, 30(16), 2785–2791. doi:10.1002/jcc.21256
 32. Guide MU. (2015) MarvinSketch User's Guide Table of Contents. <http://www.chemaxon.com/marvin>
 33. Kim S, Chen J, Cheng T, Gindulyte A, He J, et al. (2021) PubChem in 2021 : new data content and improved web interfaces. 49:1388-1395. doi:10.1093/nar/gkaa971
 34. Trott O, Olson A. (2010) AutoDock Vina: improving the speed and accuracy of docking with a new scoring function, efficient optimization and multithreading. *Journal of Computational Chemistry*, 31(2):455. doi:10.1002/JCC.21334
 35. Discovery Studio Visualizer Software, Version 4.0 (2012). <https://discover.3ds.com/discovery-studio-visualizer-download>
 36. Wallace A, Laskowski R, Thornton J. (1995) LIGPLOT: A Program to Generate Schematic Diagrams of Protein-Ligand Interactions The LIGPLOT Program Automatically Generates Schematic 2-D Representations of Protein-Ligand Complexes from Standard Protein Data Bank File Input. Vol 8. <https://academic.oup.com/peds/article-abstract/8/2/127/1561050>
 37. Shan J JC. (2020) MolOpt: A Web Server for Drug Design using Bioisosteric Transformation. *Curr Comput Aided Drug Des.* 2020;16(4):460-466. doi: 10.2174/1573409915666190704093400.
 38. Wirth M, Zoete V, Michielin O, and Sauer B. (2013) SwissBioisostere: A database of molecular replacements for ligand design. *Nucleic Acids Res.* 41(D1). doi:10.1093/nar/gks1059
 39. Rydberg P, Gloriam D, Zaretski J, Breneman C, Olsen L. (2010) SMARTCyp: A 2D method for prediction of cytochrome P450-mediated drug metabolism. *ACS Medicinal Chemistry Letters*, 1(3):96-100. doi:10.1021/ml100016x
 40. Rudik A, Bezhentsev V, Dmitriev A, Lagunin A, Filimonov D, Poroikov V. (2019) Metatox-Web application for generation of metabolic pathways and toxicity estimation. *Journal of Bioinformatics and Computational Biology.* doi:10.1142/s0219720019400018
 41. Djoumbou-Feunang Y, Fiamoncini J, Gil-de-la-Fuente A, Greiner R, Manach C, Wishart D. (2019) BioTransformer: A Comprehensive Computational Tool for Small Molecule Metabolism Prediction and Metabolite Identification. *Journal of*

- Cheminformatics, 11(1). doi:10.1186/s13321-018-0324-5
42. Daina A, Michielin O, Zoete V. (2017) SwissADME: A free web tool to evaluate pharmacokinetics, drug-likeness and medicinal chemistry friendliness of small molecules. *Sci Rep.* doi:10.1038/srep42717
 43. Xiong G, Wu Z, Yi J, Fu L, Yanhg Z, Changyu H, et al. (2021) ADMETlab 2.0: an integrated online platform for accurate and comprehensive predictions of ADMET properties. *Nucleic Acids Research*, 49(W 1), W 5 – W 1 4 . doi:10.1093/nar/gkab255
 44. Neveu E, Popov P, Hoffmann A, Migliosi, A, Bouvry P, Besson X. (2018) Structural bioinformatics RapidRMSD : rapid determination of RMSDs corresponding to motions of flexible molecules. *Bioinformatics*, 34(16), 2757–2765. doi:10.1093/bioinformatics/bty160
 45. Reva B, Finkelstein A, Skolnick J. (1998) What is the probability of a chance prediction of a protein structure with an rmsd of 6 Å? *Folding and Design*, 3(2), 141–147. doi:10.1016/s1359-0278(98)00019-4
 46. Hosfield D, Wu Y, Skene E, Hilger M, Jennings A, Snell G. (2005) Conformational flexibility in crystal structures of human 11 β -hydroxysteroid dehydrogenase type I provide insights into glucocorticoid interconversion and enzyme regulation. *Journal of Biological Chemistry*, 280(6), 4639–4648. doi:10.1074/jbc.m411104200
 47. Thomas M. (2011) Crystal structures of 11 β -hydroxysteroid dehydrogenase type 1 and their use in drug discovery. *Future Medicinal Chemistry*, 3(3), 367–390. doi:10.4155/fmc.10.282
 48. Hapman K, Holmes M, Seckl J. (2013) 11B-Hydroxysteroid Dehydrogenases Intracellular Gate-Keepers of Tissue Glucocorticoid Action. *Physiological Reviews*, 93(3), 1139–1206. doi:10.1152/physrev.00020.2012
 49. Fu H, Park J, Pei D. (2002) Peptidyl Aldehydes as Reversible Covalent Inhibitors of Protein Tyrosine. *Biochemistry*, 41(34), 10700–10709. doi:10.1021/bi0258748
 50. Johnson T, Ermolieff J, Jirousek M. (2002) Protein tyrosine phosphatase 1B inhibitors for diabetes. *Nature Reviews Drug Discovery*, 1(9), 696–709. doi:10.1038/nrd895
 51. Ala P, Gonneville L, Hillman M, Becker-Pasha M, Wei M, Reid B, et al. (2006) Structural basis for inhibition of protein-tyrosine phosphatase 1B by isothiazolidinone heterocyclic phosphonate mimetics. *Journal of Biological Chemistry* 281(43): 32784–32795. doi:10.1074/jbc.M606873200
 52. Kuang J, Chen L, Tang Q, Zhang J, Li Y, and He J. (2018) The role of Sirt6 in obesity and diabetes. *Front Physiology*. doi:10.3389/fphys.2018.00135
 53. You W, Zheng W, Weiss S, Chua K, Steegborn C. (2019) Structural basis for the activation and inhibition of Sirtuin 6 by quercetin and its derivatives. *Scientific Reports*, 9(1). doi:10.1038/s41598-019-55654-1
 54. Rahnasto-Rilla M, Tyni J, Huovinen M, Jarho E, Kulikowicz T, Ravichandran S, Bohr V. (2018) Natural polyphenols as sirtuin 6 modulators. *Scientific Reports*, (1):1-11. doi:10.1038/s41598-018-22388-5
 55. Gregory S, Hill D, Grey B, Ketelbey W, Miller T, Muniz-Terrera G, et al. (2020). 11B-Hydroxysteroid Dehydrogenase Type 1 Inhibitor Use in Human Disease—a Systematic Review and Narrative Synthesis. *Metabolism: Clinical and Experimental*. doi:/10.1016/j.metabol.2020.154246
 56. Andrews R, Rooyackers O, Walker B. (2003). Effects of the 11 beta-hydroxysteroid dehydrogenase inhibitor carbenoxolone on insulin sensitivity in men with type 2 diabetes. *The Journal of Clinical Endocrinology and Metabolism*. doi.org/10.1210/JC.2002-021194
 57. Reidenberg M. (2000). Environmental inhibition of 11 β -hydroxysteroid Dehydrogenase. *Toxicology*, 144 (1–3), 107–111. doi.org/10.1016/S0300-483X(99)00196-1
 58. Irving E. Stoker A. (2017). Vanadium Compounds as PTP Inhibitors. *Molecules* 22 (12). doi.org/10.3390/MOLECULES22122269
 59. Patel H, Dhangar K, Sonawane Y, Surana, S., Karpoomath, R, et al. (2018). In search of selective 11 β -HSD type 1 inhibitors without nephrotoxicity: An approach to resolve the metabolic syndrome by virtual based screening. *Arabian Journal of Chemistry*, 11(2), 221–232. doi.org/10.1016/j.arabjc.2015.08.003
 60. Priefer R. (2020). PTP1B Inhibitors as Potential Target for Type II Diabetes. *Current Research in Diabetes & Obesity Journal*, 14(1). doi.org/10.19080/crdoj.2020.14.555876 Conf. Ind. Eng. Oper. Manag., vol. 0, no. March, pp. 1679–1690, 2020.

Appendix A - Criteria for pharmacokinetic and physicochemical evaluation

| Property | Parameter | Empirical Decision | Results Interpretation | |
|----------------------------|--------------------------|---|---|---------------------------------|
| Absorption | P-gp inhibitor | 0-0.3: excellent; 0.3-0.7: medium; 0.7-1.0: poor | Category 0: Non-inhibitor/Non-substrate | |
| | P-gp substrate | | Category 1: Inhibitor/Substrate | |
| Distribution | GSI (HIA+) | | Category 0: >30% : Highly absorbed Category 1: <30% : Poorly absorbed | |
| | BBB permeation (BBB+) | | Category 0: BBB- Category 1: BBB+ | |
| Metabolism | Plasma Protein Binding | ≤90%: Excellent >90%: Poor | ≤90%: High therapeutic index >90%: Low therapeutic index | |
| | CYP1A2 inhibitor | | | |
| Metabolism | CYP1A2 substrate | | | |
| | CYP2C19 inhibitor | | | |
| | CYP2C19 substrate | | | |
| | CYP2C9 inhibitor | 0-0.3: excellent; 0.3-0.7: medium; 0.7-1.0: poor | Category 0: Non-inhibitor/Non-substrate | Category 1: Inhibitor/Substrate |
| | CYP2C9 substrate | | | |
| | CYP2D6 inhibitors | | | |
| | CYP2D6 substrate | | | |
| | CYP3A4 inhibitor | | | |
| | CYP3A4 substrate | | | |
| | Excretion | Renal clearance | >15 ml/min/kg: high clearance; 5-15 ml/min/kg: moderate clearance; <5 ml/min/kg: low clearance. | |
| Half-life (long half-life) | | | Category 0: short half-life Category 1: long half-life | |
| Toxicity | hERG inhibition (active) | 0-0.3: excellent; 0.3-0.7: medium; 0.7-1.0: poor | Category 0: Inactive Category 1: Active | |
| | Carcinogenicity (toxic) | | Category 0: Non-carcinogen Category 1: Carcinogen | |
| | Hepatotoxicity (toxic) | | Category 0: Non-hepatotoxic Category 1: Hepatotoxic | |
| Physicochemical Properties | LogP | | 0 to 3 log mol/L : Excellent | |
| | LogS | | -4 to 0.5 log mol/L : Excellent | |
| Violations | Lipinski | | | |
| | Ghose | | | |
| | Veber | | Percentage of compliance | |
| | Egan | | | |
| | Muegge | | | |
| | QED | | >0.67: excellent/attractive, <0.67 poor, unattractive | |
| Synthetic Accessibility | | <6: Excellent ≥6: Poor | <6: Easy to synthesize ≥6: Difficult to synthesize | |

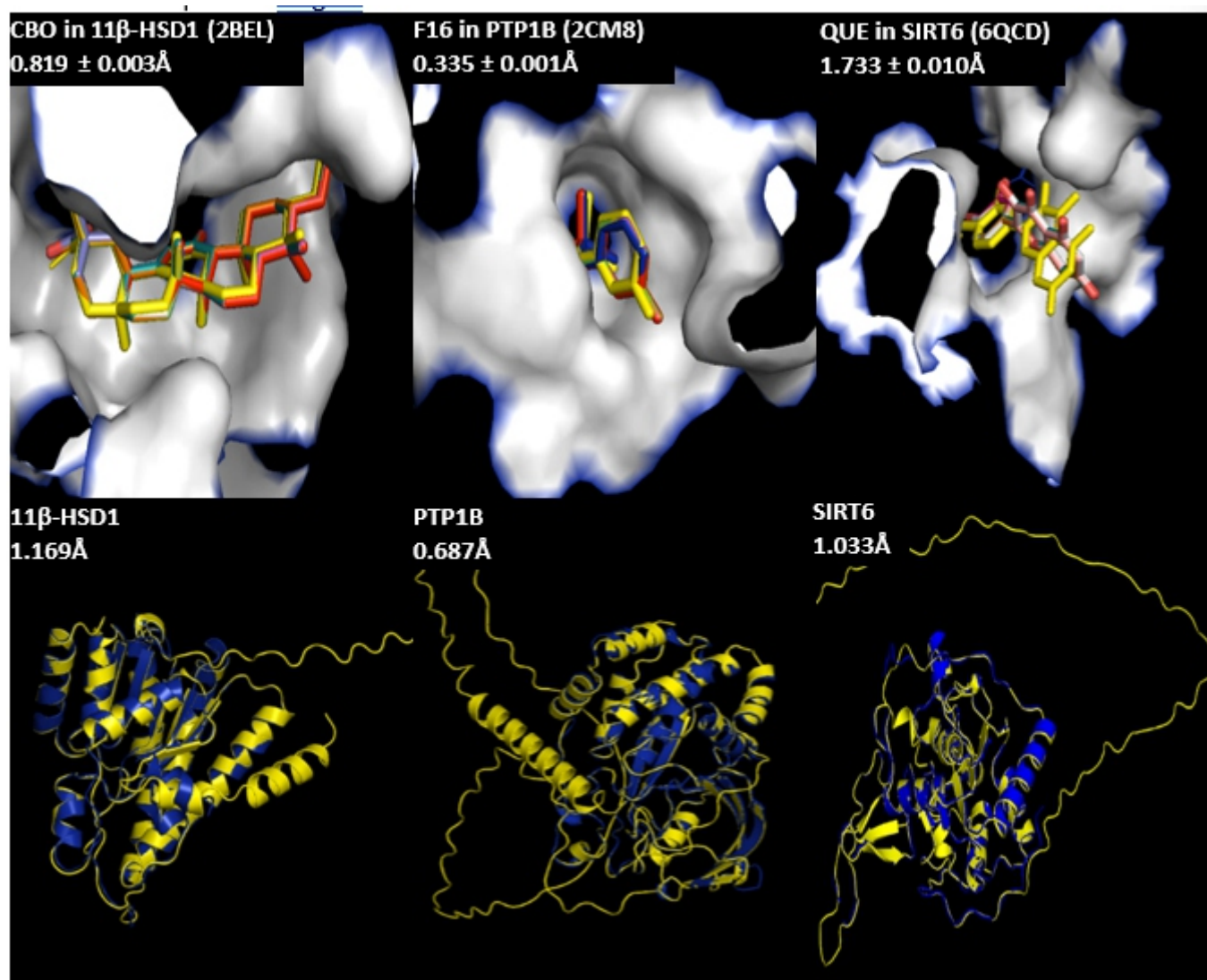
Appendix B - Grid box values

| Parameters | 11β-HSD1 | | PTP1B | | SIRT6 | |
|------------------------------|----------|--------|--------|--------|---------|---------|
| | PDB | AF2 | PDB | AF2 | PDB | AF2 |
| Center (coordinates) | | | | | | |
| X | 51.462 | 6.531 | 47.127 | 1.451 | -24.047 | -0.853 |
| Y | 5.505 | 1.605 | 15.482 | 11.154 | 26.63 | -0.327 |
| Z | -21.655 | -7.245 | 4.526 | -8.226 | 20.292 | -11.688 |
| Dimension (number of points) | | | | | | |
| X | 32 | 28 | 20 | 25 | 20 | 25 |
| Y | 25 | 25 | 20 | 25 | 20 | 25 |
| Z | 24 | 25 | 20 | 25 | 20 | 25 |

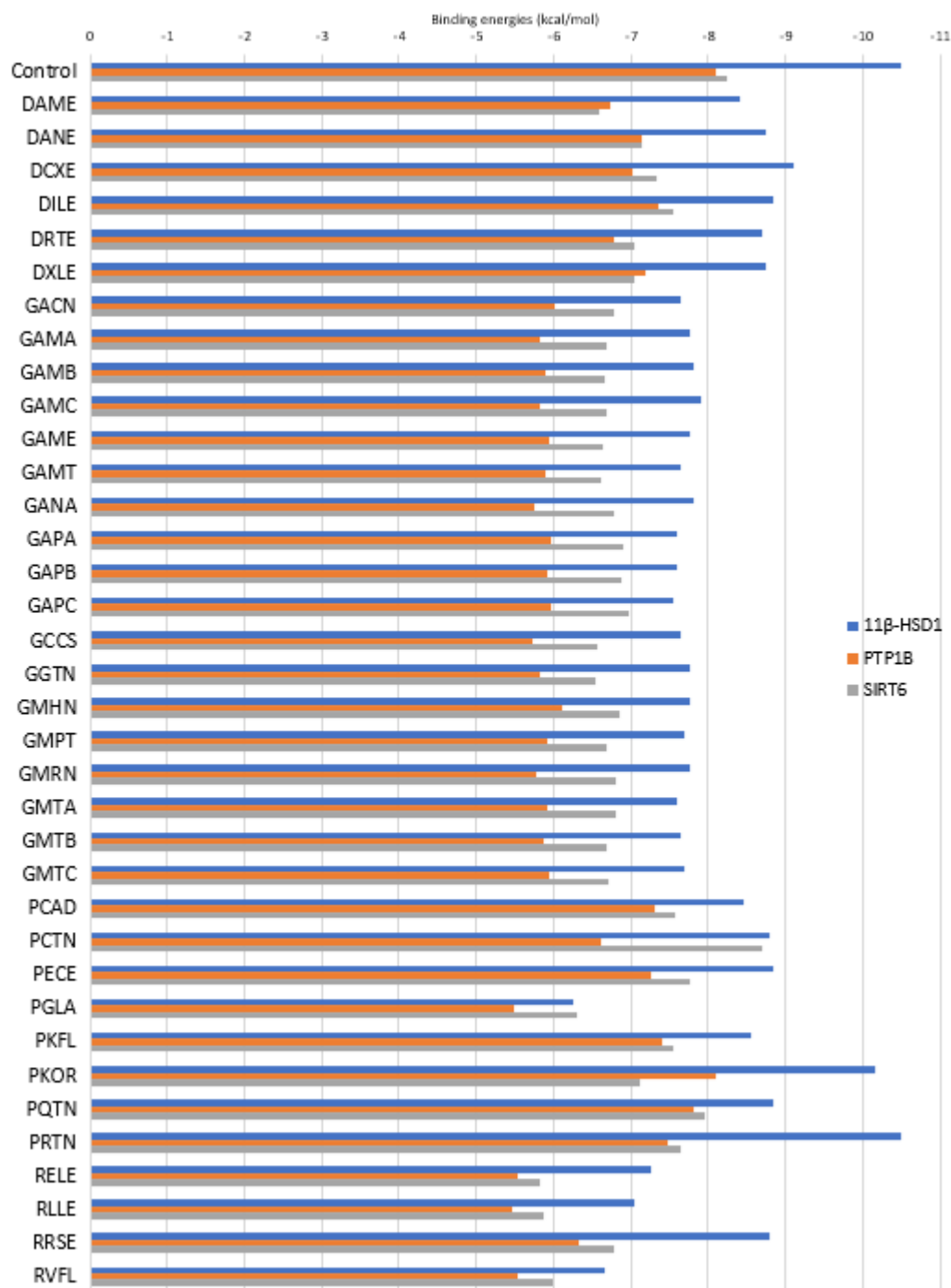
Appendix C - Reported amino acid residues of the protein targets

| Protein | Native ligand | Amino acid residues |
|----------|--|--|
| 11β-HSD1 | Carbenoxolone (CBO) | Ser170, Leu171, Ala172, Tyr 177, Tyr183, Leu217, Ala223, Ala226, Val227, Val231, Met233 |
| PTP1B | 5-(3-Hydroxyphenyl) isothiazol-3(2H)-one 1,1-dioxide (F16) | Arg024, Tyr046, Asp048, Val049, Asp181, Phe182, His214, Cys215, Ser216, Ala217, Ile219, Gly220, Arg221, Arg254, Gln262 |
| SIRT6 | Quercetin (QUE) | Ala053, Ile061, Pro062, Phe064, Phe082, Phe086, Gly111, Val115, Asp116, Met136, Met157, Ile185, Trp188 Thr213, Gly214 |

Appendix D - Superimposed redocked conformations of the bound ligands and the PDB and AF2 models of the protein targets



Appendix E - Mean binding energies of the parent compounds towards the three protein targets



Appendix F - Pharmacokinetic and physicochemical screening results of the best ligand in protein target

| Property | Parameter | 11 β -HSD1 | | PTP1B | | SIRT6 | |
|-----------------------------------|------------------------|------------------|--------|--------|--------|--------|--------|
| | | PRTN | ASM021 | PCAD | HCM004 | PECE | DSM008 |
| Absorption | P-gp inhibitor | 0.005 | 0.008 | 0.000 | 0.003 | 0.007 | 0.003 |
| | P-gp substrate | 0.997 | 0.998 | 0.558 | 0.996 | 0.004 | 0.003 |
| | GSI | 0.876 | 0.830 | 0.873 | 0.888 | 0.037 | 0.105 |
| Distribution | BBB permeation | 0.041 | 0.043 | 0.590 | 0.088 | 0.025 | 0.030 |
| | Plasma Protein Binding | 87.11% | 89.20% | 67.19% | 78.99% | 92.36% | 84.31% |
| Metabolism | CYP1A2 inhibitor | 0.121 | 0.135 | 0.036 | 0.027 | 0.393 | 0.206 |
| | CYP1A2 substrate | 0.041 | 0.066 | 0.042 | 0.064 | 0.224 | 0.111 |
| | CYP2C19 inhibitor | 0.035 | 0.046 | 0.023 | 0.036 | 0.031 | 0.025 |
| | CYP2C19 substrate | 0.048 | 0.056 | 0.053 | 0.065 | 0.054 | 0.061 |
| | CYP2C9 inhibitor | 0.018 | 0.017 | 0.016 | 0.109 | 0.323 | 0.127 |
| | CYP2C9 substrate | 0.139 | 0.140 | 0.511 | 0.267 | 0.827 | 0.579 |
| | CYP2D6 inhibitor | 0.056 | 0.073 | 0.003 | 0.007 | 0.139 | 0.100 |
| | CYP2D6 substrate | 0.129 | 0.134 | 0.156 | 0.080 | 0.310 | 0.252 |
| | CYP3A4 inhibitor | 0.039 | 0.048 | 0.030 | 0.034 | 0.371 | 0.158 |
| | CYP3A4 substrate | 0.003 | 0.006 | 0.022 | 0.089 | 0.180 | 0.307 |
| Excretion | Renal clearance | 1.502 | 1.501 | 3.251 | 12.158 | 16.512 | 14.565 |
| | Half life | 0.728 | 0.638 | 0.928 | 0.827 | 0.884 | 0.879 |
| Toxicity | hERG inhibition | 0.227 | 0.219 | 0.014 | 0.048 | 0.030 | 0.039 |
| | Carcinogenicity | 0.055 | 0.065 | 0.059 | 0.884 | 0.159 | 0.118 |
| | Hepatotoxicity | 0.083 | 0.084 | 0.122 | 0.241 | 0.093 | 0.099 |
| | Lipinski | 25% | 25% | 75% | 75% | 100% | 100% |
| Physicochemical Properties | LogP | -0.038 | 0.545 | -0.162 | 0.637 | 1.213 | 0.961 |
| | LogS | -3.742 | -3.837 | -1.198 | -2.205 | -2.720 | -2.881 |
| Violations | Ghose | 0% | 0% | 75% | 100% | 100% | 100% |
| | Veber | 50% | 50% | 50% | 50% | 100% | 100% |
| | Egan | 50% | 50% | 50% | 50% | 100% | 100% |
| | Muegge | 56% | 56% | 78% | 89% | 100% | 100% |
| | QED | 0.140 | 0.161 | 0.234 | 0.287 | 0.510 | 0.535 |
| Synthetic Accessibility | | 4.783 | 4.763 | 3.781 | 4.074 | 3.334 | 3.346 |

Reference value or the range of acceptability for each parameter can be seen Appendix A
Green (Passed); Red (Failed)

Appendix G - Two-dimensional structures of the top ligands for each target based on ADMET-physicochemical profiles

